THE INSTITUTE OF SPACE AND ASTRONAUTICAL SCIENCE
YOSHINODAI, SAGAMIHARA, KANAGAWA 229

ISAS RESEARCH NOTE

ISAS RN 563

Digital Alignment Control for the TENKO-100 DL Interferometer

E.G. Heflin , N. Kawashima

March 1995

Digital Alignment Control for the TENKO-100 DL Interferometer

E.G. Heflin[1], N. Kawashima
The Institute of Space and Astronautical Science
Yoshinodai Sagamihara, Kanagawa 229 Japan

1. Abstract

With the ever increasing digital processing rates, the application of digital feedback is becoming a feasible alternative to analog feedback systems for interferometers with targeted search frequencies of ~ 1 kHz or less. In this paper, the structure and implementation of a digital alignment control system for use with such interferometers. The digital feedback control uses an optimized infinite impulse response (IIR) filter for real-time control of the mirrors in a gravitational-wave interferometer. The system is implemented and tested on one baseline of the 100 m delay-line interferometer at ISAS, TENKO-100. The digital feedback control is then compared to the same analog feedback control for the alignment system.

2. Introduction

Due to increasing processing rates, i.e. reduced processing times, and decreasing hardware prices, the application of digital feedback control to interferometeric devices is becoming an economically and technologically feasible alternative to analog feedback. The advantages for such systems include flexible filtering (software filter), selective filtering (frequency domain filtering with Fast Fourier Transforms (FFT) for accurate point-wise gain or real-time domain filtering with infinite or finite impulse response filters (IIR and FIR)), standardized feedback control (all systems can be implemented with the same analog to digital converter (ADC), central processing unit (CPU), and digital to analog converter (ADC) interfaces), and ease of integration in a data acquisition systems (digital signals are directly recorded with the rest of the data). The disadvantages for such systems are dependent on the total processing time, $\Delta\tau$, defined as the total of ADC, CPU processing and filtering, and DAC times, and the associated Nyquist frequency cutoff as well as possible roundoff errors in data acquisition conversion (DAQ) and processing.

[1]Visiting Research Associate with NSF/JSPS Fellowship

3. The Alignment System

The digital feedback system described here is used with a previously described mirror alignment system for the TENKO-100 DL interferometer (Heflin 1994) shown in Figure 1. The difference here is in the use of digital, instead of analog, feedback control.

3.1. Control Components

Basically, the alignment control system works on the principle that small rotations of a cylindrically symmetric mirror about its transverse axis, θ and ϕ, will produce large deviations in the measured transverse positions, x and y, for reflected beam of light with long baseline. These changes in the x and y positions are detected with sensitive four-quadrant photodetectors, shown in Figure 2. Combining the output signals to give corresponding x and y positions, allows for high precision feedback control of the reflecting mirror in the linear regime.

Typical signals from the four-quadrant photodetectors are shown in Figure 3 for the time domain and in (a) of Figure 5 for the frequency domain. Note the presence of low frequency noise in the FFT spectrum for a typical photodetector signal. This low frequency noise is correlated to obvious seismic activity, esp. as the passing of cars and trucks during the day, and is evidenced from the time domain output of a typical photodetector.

3.2. Digital Components

The actual components of the digital feedback system can be divided into two general areas, hardware and software. The hardware components of the digital system include:

(1) Analog to Digital Converter (ADC): AZI-275 with 15 μs readout time for up to 16 channels. The conversion is 12 bit yielding 1.22 mV range on a typical $\pm$50 mV photodetector signal.

(2) Central Processing Unit (CPU): NEC-9801 with 25 MHz internal processing clock and a math coprocessor.

(3) Digital to Analog Converter (ADC): AZI-3302 with 10 μs output time for up to 8 channels.

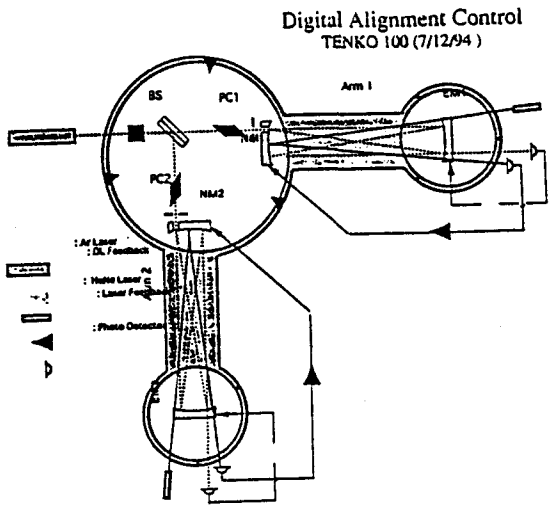

Fig. 1.— The Alignment System.
The basic alignment system consists of an external laser beam with a photodetector, a residual delay-line beam with another photodetector, and digital feedback control for the two mirrors in each baseline of the interferometer.

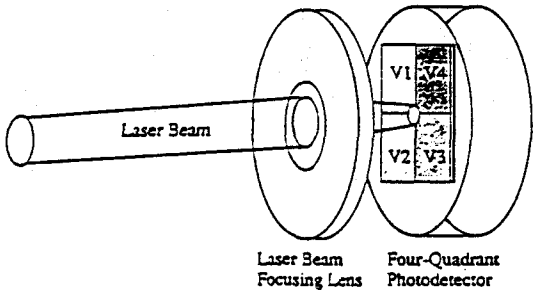

Fig. 2.— The Photodetector.
The photodetector used here is a four-quadrant type with output of a voltage from each of the four different quadrants as shown. These voltages are amplified and added or subtracted to yield signals corresponding to the x and y axis: $V_x = [(V_4 + V_3) - (V_2 + V_1)]$ and $V_y = [(V_4 + V_1) - (V_2 + V_3)]$.

The conversion is 12 bit with decoupled input voltage and output voltage.

Similarly, the software components for the digital system can be grouped into three broad areas according to their functionality in the digital feedback system.

(1) Calibration Programs: Programs used to monitor signals and perform preliminary measurements necessary for the main feedback routines. For example, the routine MON.C performs monitoring and verification of proper operation of the digital feedback system, while CAL.C performs the essential calibration measurements of the photodetectors, i.e. m and b determination, for use with the main feedback routine.

(2) Feedback Programs: Programs used for conversion (ADC and DAC), processing, and filtering data as part of the real-time feedback. For example, the present system combines all DAQ and IIR filtering into one single routine, DCON.C. This approach generally reduces the total feedback processing time, $\Delta\tau$.

(3) Utility Programs: Programs used for special purposes studies of the digital feedback system. For example, BODE.C is used for swept sine wave applications and filter optimization studies.

Run time for the different programs range from $\sim$ 0.2 ms for MON.C and BODE.C to $\sim$ 0.9 ms for DCON.C. Since the total processing time is the single most important limiting factor in system performance, it is important to realize that Calibration and Utility Programs are, by definition, not used during real-time applications. Therefore, all limitations of the present system due to the total processing time are due to the main feedback program, DCON.C.

Implementation of the digital feedback system is accomplished in four steps: manual calibration, digital monitoring, digital calibration, and finally digital feedback. First, each of the four photodetectors is manually set and calibrated so that the beam spot scan axis are aligned with four-quadrant axis of the photodetector and the beam spot is centered on the center of the four-quadrant center of the photodetector. Notice that the first condition reduces the cross correlation of the mirror motions, R and P, and

the photodetector axis, X and Y (the off-diagonal elements in the slope, m, matrix), while the second condition correlates the origin of the beam spot with the origin of the measured X and Y. This is important since the photodetector sensitivity decreases away from the center due to geometrical considerations and shot noise. The preamplifiers for the photodetectors are checked and set to give an output voltage in the range of $\pm$ 50 mV. Second, correct operation of the DAQ conversion is performed by comparing the analog and digital signals with two oscilloscopes. Third, the digital calibration of each of the four photodetectors is accomplished by seperately varying the R and P for its corresponding mirror and observing the response in the X and Y output for that photodetector. Since even in the linear regime there may be possible correlation of the X and Y signals due to the R and P motions of the mirror, both responses must be recorded to determine the slopes, m, and intercepts, b, of correlation. Fourth, the calibration constants are incorporated into the main digital feedback routine, DCON.C, and the other digital filter parameters are optimized by a semi-trial and error method. After optimization, the digital feedback system is operated and the response is monitored and recorded.

4. Theory

The objective in alignment control is to align the main interferometer laser beam to the optical components of the interferometer system, e.g. the near and far mirror in each baseline of the interferometer. For the simple pitch and roll motions of TENKO-100 mirrors, this objective can be translated into the following two stability conditions:

(1) $\vec{n_2} \bullet \hat{j} = 1$ - The near mirror must be perpendicular to the direction of an external laser beam.

(2) $\vec{n_2} \bullet \vec{n_1} = -1$ - The end mirror must be perpendicular to the near mirror at all times.

The first condition provides absolute referential control for each baseline of delay-line interfermoter through the near mirror, while the second provides relative control for each baseline of the delay-line interferometer through the far mirror. In practice, these conditions are meet by assuring that the laser beam light is always centered on the photodetector. Conceptually this is accomplished through three successive steps in the digital feedback system corresponding to three successive transformations of the X and Y signals for feedback control.

4.1. Digital Control

In the linear regime, the first of the transformations relates the photodetector input signals, $X(V_x$ and $Y(V_y)$ and the unfiltered feedback output signals $R(V_r)$ and $P(V_p)$.

$$\begin{pmatrix} R \\ P \end{pmatrix} = \begin{bmatrix} m_{R_x} & m_{R_y} \\ m_{P_x} & m_{P_y} \end{bmatrix} \begin{pmatrix} X \\ Y \end{pmatrix} + \begin{bmatrix} b_{R_x} & b_{R_y} \\ b_{P_x} & b_{P_y} \end{bmatrix}$$

Here, the slopes, m, and intercepts, b, are determined by digital calibration, as mentioned before, prior to feedback control. The slopes are found by varying the R and P for the mirror control input and measuring, simultaneously, the photodetector response in X and Y. The intercepts correspond, roughly, to the "origin" of the beam position on the face of the photodetector after manual calibration.

The next step before converting the digital signal into an output feedback signal involves filtering. The approach taken here is to separate the important aspect of frequency response from the gain response in the filtering process. The frequency response signal, R_{filter} and P_{filter}, is determined first using one of two filtering schemes discussed in the Filtering Section. Although no preference for filtering was taken *a priori*, it was essential that the filtering be completed in real-time with the system. For this reason, two distinct methods for filtering were tried, i.e. frequency domain with FFTs and time domain with IIR, only the latter was found suitable for the particular CPU used. Hence, in transformation notation

$$\begin{pmatrix} R_{filter} \\ P_{filter} \end{pmatrix} = \begin{bmatrix} F_{R_x}(t) & 0 \\ 0 & F_{P_y}(t) \end{bmatrix} \begin{pmatrix} R \\ P \end{pmatrix}$$

In practice, an approximate gain for the digital feedback system is used to guide the trial and error in optimizing the system for the appropriate filter gain. Thus, the final digital feedback control transformation with filtering and gain takes the form

$$\begin{pmatrix} R_{out} \\ P_{out} \end{pmatrix} = \begin{bmatrix} G_{R_x} & G_{R_y} \\ G_{P_x} & G_{P_y} \end{bmatrix} \begin{pmatrix} R_{filter} \\ P_{filter} \end{pmatrix}$$

Notice that in an analog system, this three step matrix approach is automatically performed in one fell swoop by control of the filtering process, i.e. frequency gain and phase.

4.2. Filtering

Two different approaches for digital filtering were considered and implemented on the present system: frequency domain filtering with Fast Fourier Transformations (FFT) and time domain filtering using infinite impulse response filtering (IIR). The basic ideas of filtering in a discrete digital world are founded in the continuous analog world with certain important differences. Two important differences are that the digital signals are discrete in both time and amplitude. This discreteness in time gives rise to an effective cutoff frequency for application of the system, i.e. the Nyquist frequency $f_{Nyquist} \approx \pi/\Delta\tau$, while the discreteness in amplitude gives rise to possible roundoff errors.

The first approach to filtering involved a FFT to transform the signals to the frequency domain and perform the actual filtering there (Numberical Recipes). Briefly, this method used four points from the previous output signal of the time domain and added four fictitious future points taken as zero, for a total of eight points for the FFT. The eight points are Fourier transformed according to

$$\begin{aligned} H(f_n) &= \int_{-\infty}^{+\infty} h(t) e^{2\pi i f_n t} \Delta\tau \approx \sum_{k=0}^{N-1} h_k e^{2\pi i f_n t_k} \Delta\tau \\ &= \Delta\tau \sum_{k=0}^{N-1} h_k e^{2\pi i k n/N} \approx \Delta\tau H_n \end{aligned}$$

where $t_k \equiv k\Delta\tau$ and $f_n \equiv \frac{n}{N\Delta\tau}$ has been assumed. As mentioned, the actual transformation implemented was an FFT using standard bit reversal techniques to reverse the number of operations for the from N^2 to $Nlog_2N$, and thus dramatically reducing processing time. The eight points are then filtered in the frequency domain allowing very precise filtering in an extremely flexible format. Finally, the eight points are inverse Fourier transformed according to

$$h_k = \frac{1}{N} \sum_{n=0}^{N-1} H_n e^{-2\pi i k n/N}$$

and, assuming minimal aliasing, the next point in the time domain is used for feedback control. Unfortunately, implementation of this filtering approach required total processing times in the order of 10's of ms using the 25 MHz machine described above. This was therefore considered unacceptably long and a real-time solution was sought.

The second approach to filtering used a real-time recursive filter to perform filtering in the time domain (Digital Filters). The basic idea is assumes that up to the given point in time the output, x_k, is some simple function of the input, y_k.

$$\sum_{n=0}^{N} c_n x_{k-n} = \sum_{n=0}^{N} d_n y_{k-n} = y_k + \sum_{n=1}^{N} d_n y_{k-n}$$

Assuming a linear periodic system with

$$\begin{aligned} x_k &= V_{in} e^{-\omega k} \equiv V_{in} z^{-k} \\ y_k &= V_{out} e^{-\omega k} \equiv V_{out} z^{-k} \end{aligned}$$

leads naturally to a rational expression for the transfer function

$$\begin{aligned} \mathcal{H}(\omega) &\equiv \frac{V_{out}}{V_{in}} = \frac{\sum_{m=0}^{M} c_m x_{k-m}}{1 + \sum_{n=1}^{N} d_n y_{k-n}} \\ &= \frac{\sum_{m=0}^{M} c_m e^{-\omega m}}{1 + \sum_{n=1}^{N} d_n e^{-\omega m}} = \frac{\sum_{m=0}^{M} c_m z^{-m}}{1 - \sum_{n=1}^{N} d_n z^{-n}} \end{aligned}$$

where $M \neq N$, necessarily and for convenience, we have redefined d_n as $-d_n$.

Examples of IIR filters actually used include a hybrid of a highpass filter with one zero for filtering R,

$$\begin{aligned} \mathcal{H}(\omega) &\equiv \left(\frac{\omega}{\omega - ia}\right)\left(\frac{ib}{\omega - ib}\right) \\ &= \frac{\frac{-b}{(1+a)(1+b)} + \frac{-b}{(1+a)(1+b)} z^{-1}}{1 - \frac{(1+a)(1-b)+(1-a)(1+b)}{(1+a)(1+b)} z^{-1} + \frac{(1-a)(1-b)}{(1+a)(1+b)} z^{-2}} \end{aligned}$$

From which it is easily seen that

$$\begin{aligned} c_0 &= \frac{-b}{(1+a)(1+b)} \\ c_1 &= 0 \\ c_2 &= \frac{-b}{(1+a)(1+b)} \\ d_1 &= \frac{(1+a)(1-b)+(1-a)(1+b)}{(1+a)(1+b)} \\ d_2 &= \frac{(1-a)(1-b)}{(1+a)(1+b)} \end{aligned}$$

A similar one pole IIR filter was also used for filtering P. Once the coefficients for the digital filter have been specified, a swept sine can be performed to produce a Bode Diagram in exact analogy to the analog approach as shown in Figure 4.

From the Bode diagram, the basic Nyquist frequency cutoff can be measured as the high frequency limit in response to a high pass filter. This is seen to be approximately 1 kHz implying a total DAQ "sampling" time of 1 ms. This is also the basis for the sampling time in the optimization procedure for the digital filter.

5. Results

The digital feedback control system was implemented for one baseline of the the TENKO-100 DL interferometer. The goal in developing the digital system was to operate it as a standalone feedback control system as well as test the system against an existing operational analog feedback control system (Heflin 1994).

Results from the standalone operation are shown in (b) of Figure 5 for the frequency domain. The spectrum shows improvement over the open-loop system, also shown in (a) of Figure 5, from 14 dB to 2 dB in the desired frequency range from 1 to 11 Hz for X (R) and improvement from 22 dB to 9 dB in the desired frequency range from 1 to 11 Hz for Y (P). The time domain spectrum, shown in (b) of Figure 6, also indicates effective reduction of the amplitudes for the seismically induced noises from passing cars and trucks. The system was also observed to be very stable over extended periods of time, e.g. $\delta\tau > 1$ hr.

The results from the direct comparison with analog system are shown in (c) of Figure 5 for frequency domain. The spectrum demonstrates similar gain over the open-loop system, also shown in (a) of Figure 5. The analog system affords slightly better noise reduction at the lower frequencies of interest, from 9 dB to 3 dB in the desired frequency range from 1 to 11 Hz for X (R) and improvement from 12 dB to 4 dB in the desired frequency range from 1 to 11 Hz for Y (P); however, at the higher frequencies the digital feedback system outperforms the analog system. The time domain spectrum, shown in (c) of Figure 6, also indicates comparable effectiveness in the reduction of the amplitudes for the seismically induced noises from passing cars and trucks. In comparing the stability over time, both the analog and digital feedback systems performed without significant deterioration in characteristics over periods greater than 1 hr.

6. Conclusion

In summary, the results from the digital feedback system described in this paper indicate that digital feedback control for application to interferometer systems with targeted search frequencies of $\sim$ 1 kHz or less is a feasible alternative to analog feedback systems. It has been shown to reproduce many of the same desirable features as the analog systems, including functionality, reduction in seismic noises of up to 25 dB in the 1 to 11 Hz range, and stable operation for over 1 hr. Although the structure and implementation of the system described here are specific to the TENKO-100 DL interferometer system, it should not be difficult to adapt such techniques to other types of feedback control systems up to $\sim$ 1 kHz.

REFERENCES

Heflin, E.G., *Alignment Control for the TENKO-100 Delay-Line Mirrors*, Gravitational-Wave Antenna Symposium, Mitaka, Japan, October 1994.

Flannery, B., Press W., Teulkolsky, S., and Vetterling, W. 1989, Numberical Recipes; The Art of Scientific Computing, Cambridge University Press.

Hamming, R.W. 1989, Digital Filters, 3rd Edition, Prentice Hall.

This 2-column preprint was prepared with the AAS LaTeX macros v3.0.

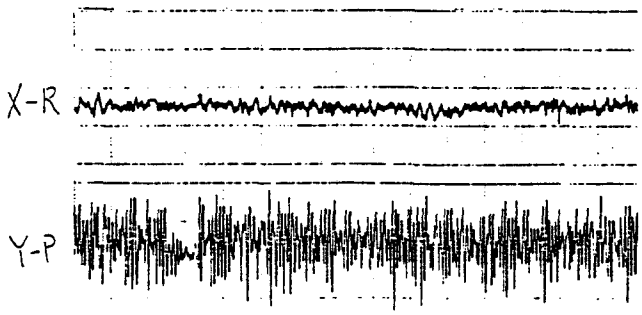

Fig. 3.— Photodetector Signal
The variation spectrum in the time domain for a typical output from a photodetector is shown on top for X (R) and on the bottom for Y (P). The most dynamic signal, largest variation, corresponds to the Y of the photodetector or the P motion of the corresponding mirror. Notice the accumulative effect of the passage of cars and trucks with the low frequency time variations of the photodetector signal. The time axis is 1 cm ≡ 12 s and the amplitude axis 1 cm ≡ 10 mV.

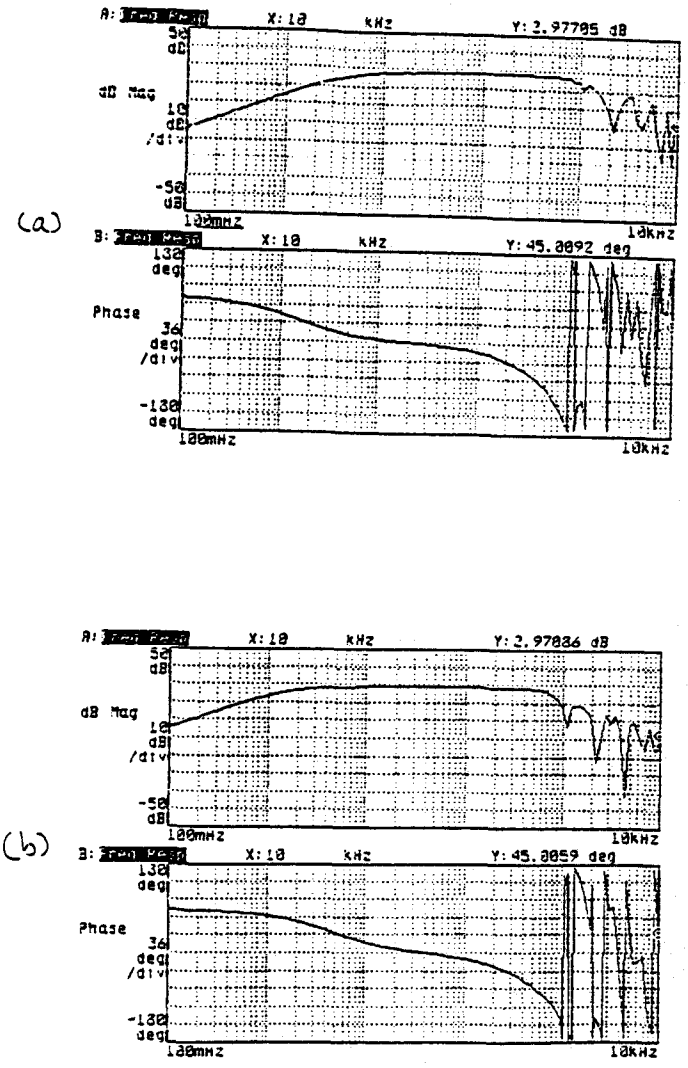

Fig. 4.— IIR Digital Filtering Response
Shown in (a) is the IIR digital filter response for the R control, while shown in (b) is the IIR digital filter response for the P control. Notice the Nyquist frequency cutoff at approximately 1 kHz implying a total DAQ "sampling" time of 1 ms.

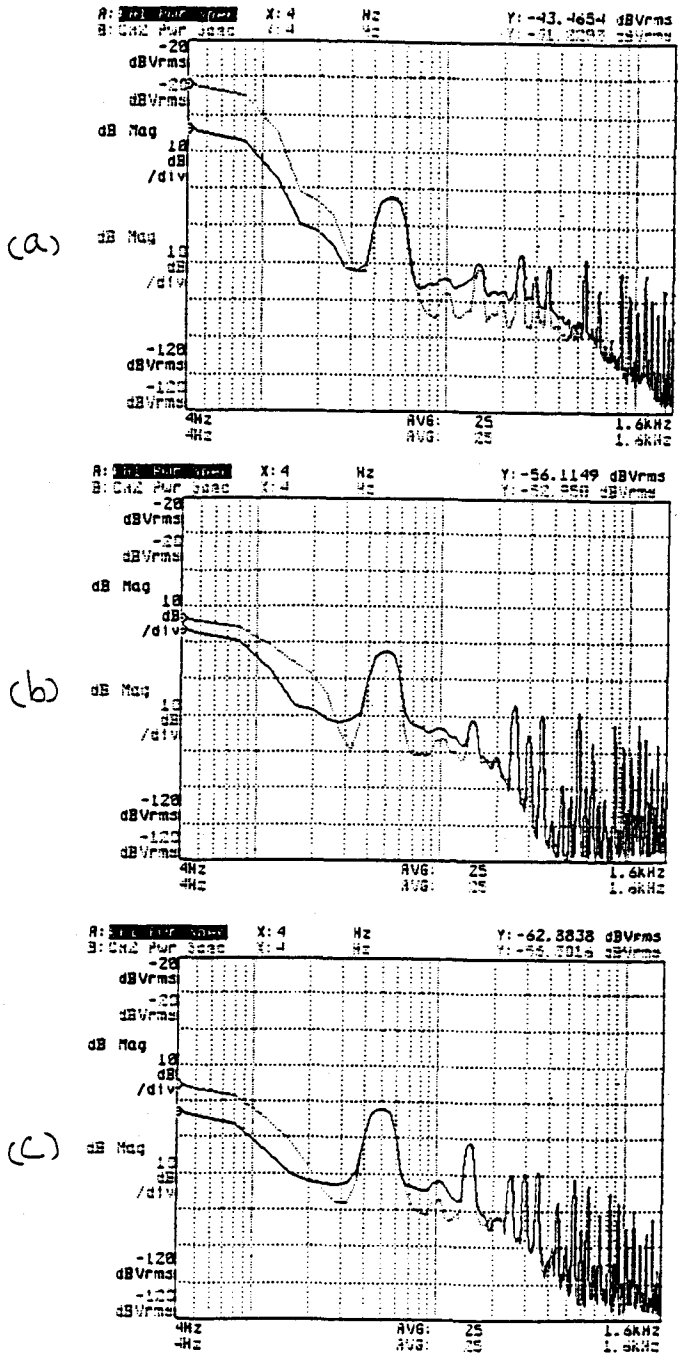

Fig. 5.— Frequency Domain: Power Spectra
Shown in (a) is the open-loop power spectrum in the frequency domain for one of the four laser-photodetector componenets of the alignment system. Shown in (b) is the power spectrum in the frequency domain for the same components of the mirror alignement control using digital feedback. Finally, shown in (c) is the like power spectrum using analog feedback control. In all spectra, the dark curve corresponds to the response for the R (X) control, while the light curve corresponds to the response for the P (Y) control. Notice, the marked improvement in response in the frequency range of 4 to 11 Hz for both the digital and analog feedback systems.

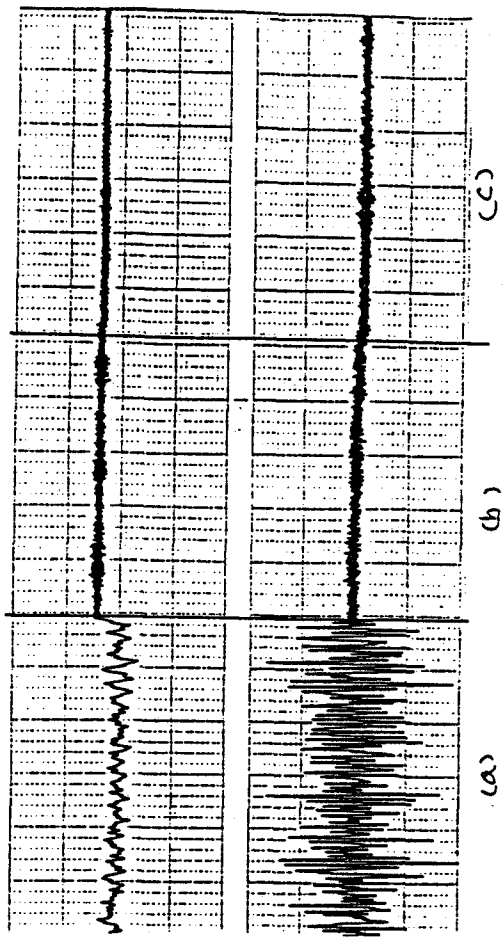

Fig. 6.— Time Domain: Variation Spectra
The variation spectra for one laser-photodetector componenet of the alignment system is shown in (a) alone, in (b) with digital feedback, and in (c) with analog feedback. The top portion is the spectrum for X (R), while the bottom spectrum is that for Y (P). Again, the time axis is 1 cm ≡ 12 s and the amplitude axis 1 cm ≡ 10 mV.